XII International Conference on Computational Plasticity. Fundamentals and Applications
COMPLAS XII
E. Oñate, D.R.J. Owen, D. Peric and B. Suárez(Eds)

DYNAMICS OF STRUCTURAL DEFECTS AND PLASTICITY: MODELS AND NUMERICAL IMPLEMENTATION FOR DYNAMICAL PROBLEMS

ALEXANDER E. MAYER[*], ELIJAH N. BORODIN[†,†††], VASILIY S. KRASNIKOV[††,†††] AND POLINA N. MAYER[†††]

[*,†††] Department of Physics, Chelyabinsk State University (CSU)
Bratyev Kashirinykh str. 129, 454001 Chelyabinsk, Russia
e-mail: mayer@csu.ru, mayer.al.evg@gmail.com; polina.nik@mail.ru; www.csu.ru

[†] Institute of Problems of Mechanical Engineering RAS (IPME RAS)
V.O. Bolshoj pr. 61, 199178 St. Petersburg, Russia
e-mail: elbor7@gmail.com; www.ipme.ru

[††] Department of Physics, Shouth-Ural State University (SUSU)
Lenina av. 76, 454080 Chelyabinsk, Russia
e-mail: vas.krasnikov@gmail.com; www.susu.ac.ru

Key words: High-rate Plasticity, Dislocations, Grain Boundaries, Localization of Plastic Flow, Metals, Molecular Crystals.

Abstract. We report the plasticity model with explicit description of kinetics of the material defects (dislocations, grain boundaries). This method becomes especially effective for computation of the dynamical deformation of materials at high strain rates because it allows for a simple accounting of the strain rate effects. The equation system is written out and discussed; its implementation is demonstrated for the problem of the plastic flow localization.

1 INTRODUCTION

Numerical investigation of different dynamical problems demands for the wide-range constitutive equations with description of the material plasticity in a wide range of strain rates. It is well known, that dynamics of structural defects provides the mechanism of plastic deformation in solids; interaction between the defects and their inertness determine the shear strength of the material. Therefore, the constitutive equation based on the dynamics and kinetics of defects (dislocations, grain boundaries, micro-twins) seems to be the most natural way of the plasticity description. Difficulties caused by additional constants can be overcome, partially due to involvement of the molecular dynamics simulation results [1], and partially due to appropriate theoretical consideration.

In this report, we discuss the dislocation plasticity model [1-3] for mono- and polycrystals and the grain boundary sliding model for plasticity of submicro- and nonocrystalline materials [4-6]. Application of these models to computations of plastic flow is described. Applicability

of the dislocation plasticity model is demonstrated for a number of metals, as well as for molecular crystals. Features of the plastic flow at the high-speed collision of ultra-thin metal plates are investigated [3]. The Hall-Petch relation is analyzed for polycrystalline materials in the quasi-static and dynamical loading conditions. The plastic flow localization is investigated on the basis of the model [7].

2 MATHEMATICAL MODEL

Total plastic deformation of polycrystalline metals is supposed to be a result of the combined action of two competing effects, namely, the dislocation motion and the sliding along the grain boundaries. According to this viewpoint, the plastic deformation tensor w_{ik} is represented by the sum $w_{ik} = w_{ik}^{\mathrm{D}} + w_{ik}^{\mathrm{gb}}$, where w_{ik}^{D} is the part of plastic deformation caused by the dislocation motion, and w_{ik}^{gb} is the part caused by the grain boundary sliding. The dislocation plasticity [1-3] and the grain boundary sliding [5-6] models are used here for determination of w_{ik}^{D} and w_{ik}^{gb} correspondently. The particular case of monocrystals corresponds to $w_{ik}^{\mathrm{gb}} = 0$. Full model consists of the continuum mechanics equations [8] supplemented by the equations for dynamics and kinetics of dislocations and by the equations for time derivatives of w_{ik}^{D} and w_{ik}^{gb}. The common part of the model, traditionally, consists of the next three conservation laws: the continuity equation

$$\frac{1}{\rho}\frac{d\rho}{dt} = -\sum_{k=1}^{N}\frac{\partial v_k}{\partial x_k}, \tag{1}$$

the equation of substance motion

$$\rho\frac{dv_i}{dt} = -\frac{\partial P}{\partial x_i} + \sum_{k=1}^{N}\frac{\partial S_{ik}}{\partial x_k}, \qquad i = 1,\ldots,N, \tag{2}$$

and the energy conservation law

$$\rho\frac{dU}{dt} = \frac{P}{\rho}\frac{d\rho}{dt} + \sum_{i=1}^{N}\sum_{k=1}^{N} S_{ik}\frac{dw_{ik}}{dt}, \tag{3}$$

where N – number of dimensions in the treated problem, indexes i,k,l numerate the space directions. In Eqs. (1)-(3): ρ is the substance density; v_i is the components of velocity vector; x_i are the Cartesian coordinates; P is the pressure, which is determined from the wide-range equation of state $P = P(\rho,U)$ [9,10]; S_{ik} is the tensor of stress deviators, which characterizes the shear stresses; U is the internal energy.

The generalized Hooke law [8] with accounting of the plastic strain w_{ik} is used for determination of the stress deviators:

$$S_{ik} = 2G\left[u_{ik} - (1/3)u_{ll}\cdot\delta_{ik} - w_{ik}\right], \tag{4}$$

where G is the shear modulus, data of papers [11,12] were used for the shear modulus

dependence on temperature and pressure $G(T,P)$; δ_{ik} is the bivalent mixed tensor; u_{ik} is the geometrical deformation, induced by the macroscopic motion of substance. It is determined by the next equation:

$$\frac{du_{ik}}{dt} = \frac{1}{2}\left[\frac{\partial v_i}{\partial x_k} + \frac{\partial v_k}{\partial x_i}\right] + \Omega_{ik}, \tag{5}$$

The term Ω_{ik} accounts for the rotation of matter [13], which is essential for 2D or 3D case.

The plastic strain tensor of the dislocation plasticity w_{ik}^{D} can be found from the generalized Orowan equation [14]:

$$\frac{dw_{ik}^{\mathrm{D}}}{dt} = -\sum_{\beta} \frac{1}{2}\left(b_i^{\beta} n_k^{\beta} + b_k^{\beta} n_i^{\beta}\right) V_{\mathrm{D}}^{\beta} \rho_{\mathrm{D}}^{\beta} + \omega_{ik}^{\mathrm{D}}, \tag{6}$$

where index β numerates the slip systems of dislocations in the material, which is characterized by the Burgers vector b_i^{β} and by the normal n_i^{β} to the slip plane; $\rho_{\mathrm{D}}^{\beta}$ is the dislocation density in corresponding slip system; V_{D}^{β} is velocity of these dislocations relative to the substance. The term ω_{ik}^{D} in the Eq. (6) takes into account the change of components w_{ik}^{D} in the laboratory system of coordinates due to the substance rotation.

The core of the dislocation plasticity model [2,3] consists of the next two equations: the equation of dislocations motion

$$m_0 \xi_{\beta}^3 \frac{\mathrm{d}V_{\mathrm{D}}^{\beta}}{\mathrm{d}t} = \left[\sum_{i=1}^{N}\sum_{k=1}^{N} S_{ik} b_i^{\beta} n_k^{\beta} \pm \frac{1}{2} bY\right] - B\xi_{\beta}^3 V_{\mathrm{D}}^{\beta}, \tag{7}$$

and the kinetics equation

$$\frac{d\rho_{\mathrm{D}}^{\beta}}{dt} = \frac{0.1}{\varepsilon_{\mathrm{D}}}\left\{2B \cdot c_{\mathrm{t}}^2 \cdot \left[\xi_{\beta} - 1\right] + b \cdot Y \cdot \left|V_{\mathrm{D}}^{\beta}\right|\right\} \cdot \rho_D^{\beta} - k_a b \cdot \left|V_{\mathrm{D}}^{\beta}\right| \cdot \left(\rho_{\mathrm{D}}^{\beta}\right)^2, \tag{8}$$

where $\xi_{\beta} = 1/\sqrt{1-\left(V_D^{\beta}/c_{\mathrm{t}}\right)^2}$; $c_{\mathrm{t}} = \sqrt{G/\rho}$ is the transverse sound speed of the material; $m_0 \approx 10^{-16}$ kg/m is the rest mass of dislocations; Y is the static yield strength; k_a is the annihilation factor; B is the phonon friction coefficient, it describes the resistance to the dislocation motion [15]; $\varepsilon_{\mathrm{D}} \approx 8\,\mathrm{eV}/b$ is the energy of the dislocations formation per unit length; b is the modulus of Burgers vector of dislocations.

The plastic strain tensor connected with the grain boundary sliding is determined as follows [4-6]:

$$\frac{dw_{ik}^{\mathrm{gb}}}{dt} = \frac{1}{2G\,\mathrm{T}} \sum_{\alpha} \tau_i^{\alpha} n_k^{\alpha} \left(\sum_{l=1}^{N}\sum_{m=1}^{N} S_{lm} \cdot \tau_l^{\alpha} n_m^{\alpha} - y_b\right) + \omega_{ik}^{\mathrm{gb}}, \tag{9}$$

where index α numerates possible planes of grains sliding, which are characterized by the normal n_i^{α}; τ_i^{α} is the direction of maximal shear stresses in the α-plane; T is the relaxation

time and y_b is the threshold stress for sliding [6]; ω_{ik}^{gb} takes into account the change of w_{ik}^{gb} due to the substance rotation [13].

Eqs (1)-(8) were solved numerically with use of the computer program CRS, written by A.E. Mayer. Sub-problem of the substance dynamics (Eqs (1)-(3)) were solved by a modification of the numerical method proposed by A.P. Yalovets [16]. All other equations were solved by Euler method with varied time step.

3 HIGH-SPEED COLLISION OF METALLIC PLATES

Collision of metallic plates is a widespread experimental technique for investigation of the shock wave propagation through the material, the dynamical plasticity and the spall effects [17-20]. The striker plate is accelerated by various methods (gas gun, explosion) and hits the target plate of the investigated material. Geometry of experiment – high transversal dimensions of plates in comparison with thickness – lets one to use the one-dimensional approximation (the uniaxial loading) in the analysis and simulations.

3.1 Verification of the model

Time profiles of the backside velocity of the target plate are experimentally registered with use of laser Doppler velocimeters [17,18]. These profiles contain all required information about dynamical plasticity of the material as well as about spall strength, polymorphic phase transitions, etc. [17,18]. Comparison of calculated profiles with the experimentally measured is a direct test for verification of the plasticity model. Such verification had been made for a number of pure metals: aluminum, copper, titanium, iron, nickel [2,3] and for alloys, including Al-Cu alloy [21]. Fig.1 shows an example of such comparison for collision of aluminum plates at two different initial temperatures of the target plate.

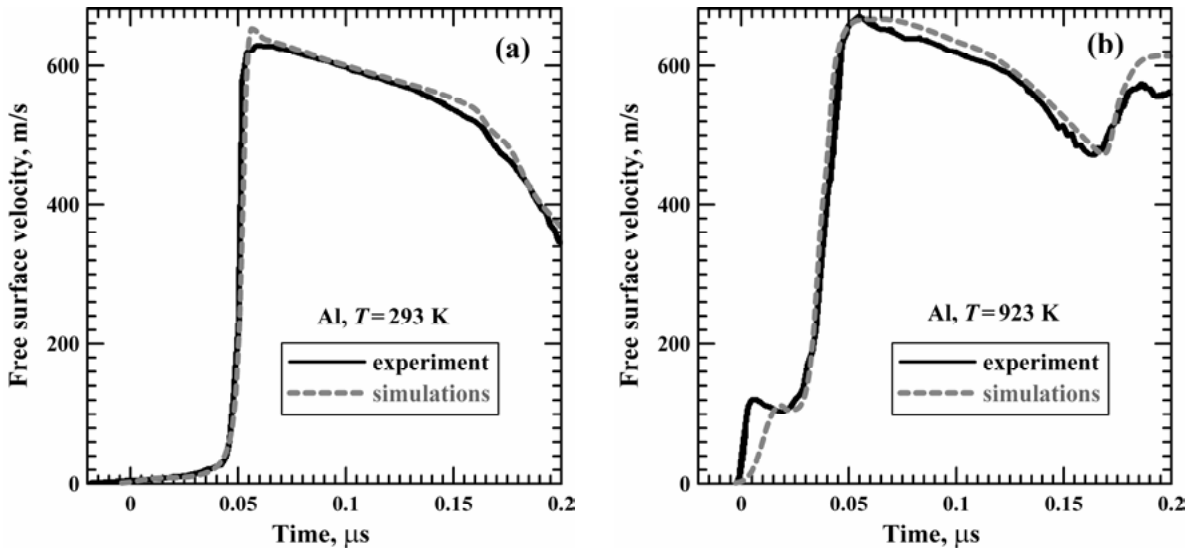

Figure 1: Time profiles of the free surface velocity of the 2.9-mm-thick aluminum single crystals at initial temperature (a) 293 and (b) 923 K impacted by the 0.4-mm-thick aluminum striker with the velocity of 680 m/s. Solid line – experimental data [19], dashed line – calculation results [3].

The striker is usually thinner than the target; the collision of plates creates the shock wave followed by the unloading wave, which is formed after reflection from the free surface of striker. The wave's attainment of the back surface is registered through velocity change. On Fig.1, the elastic precursor precedes the plastic shock-wave front and initiates initial velocity rise; the form and amplitude of the precursor are determined the strain rate and by the temperature: it is substantially defers for the considered temperatures. The unloading wave follows the shock wave and reduces the free surface velocity; its form is also determined by the metal plasticity. The reflection of the compression pulse from the rear surface generates the second unloading wave; superposition of two unloading waves creates tensile stresses and initiates the spall fracture, which is indicated through a spall pulse on curves in Fig.1(b). The simulation of spall is beyond the scope of present work and has been done with use of [3,22].

3.2 Initial stage of collision, superelastic waves

The molecular dynamics simulations [23] and femtosecond laser pulse experiments [24,25] indicate an existence of superelastic shock waves those are the elastic precursors of very high amplitude – much higher than the dynamic elastic limit. It was the reason to investigate the formation and initial evolution of the elastic precursor by example of aluminum with us of the described plasticity model. Twining is suppressed in aluminum; therefore one can expect that the dislocations dynamics control plasticity even at high shear stresses. Symmetric impact of two monocrystalline aluminum plates has been simulated in paper [3] at varied relative velocity of collision. The results for relative velocities 0.5 and 2 km/s are presented in Fig.2.

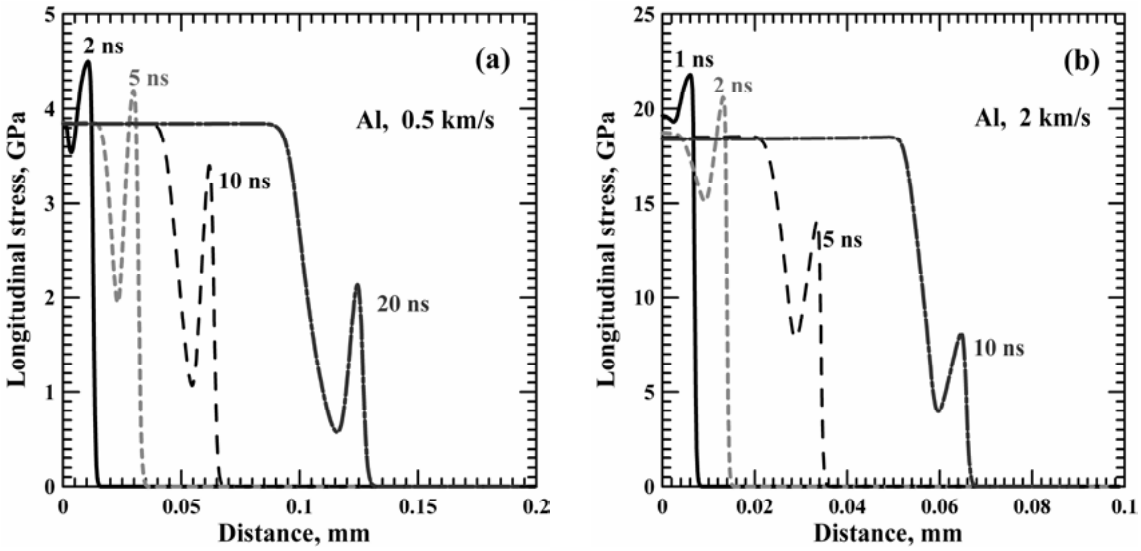

Figure 2: Formation and initial evolution of elastic precursor of the shock wave in aluminum monocrystal under symmetric impact with relative velocity of collision (a) 0.5 and (b) 2 km/s [3]. Left half of distributions of longitudinal stress is shown at different time moments.

After the impact, an initial structure of stresses splits into the elastic precursor and the plastic shock-wave front; this differentiation takes up to several nanoseconds. The initial amplitude of the elastic precursor is equal to the amplitude of the plastic shock, but it rapidly

decreases on the time scale of tenths of nanoseconds. Initial propagation velocity of the precursor is much higher than the longitudinal sound velocity c_l, which is the limit of the elastic wave velocity at low precursor amplitude. This allows the precursor to run away from the plastic shock front even at the plastic shock velocity higher than c_l; the plastic shock wave overtakes the precursor later, when the latter's amplitude decreases, and the precursor transforms into a kink on the plastic shock front. One can conclude that the described plasticity model confirms the formation of the superelastic shock wave.

4 PLASTICITY OF MOLECULAR CRYSTALS

Initially formulated and verified for metals, the described dislocation plasticity model had been further generalized on another type of materials – the molecular crystals. Various energetic materials are an essential example of the molecular crystals. The dislocation gliding is the main plasticity mechanism of the molecular crystals of energetic materials. In contrast to metals, the molecular crystals have larger value of the Burgers vector – of about $(0.5 \div 0.6)$ nm and very strong anisotropy of properties of single monocrystals. Fig.3 shows the results of the dislocation plasticity model implementation in comparison with experiments [26]. In the experiments [26], the flat shock wave is generated by impact of aluminum plate on the anvil of Kel-F 81, and thereafter passes into the RDX sample; velocity of boundary between the RDX and the LiF window is registered. As one can see, the plasticity model allows describing of the elastic precursor height and form.

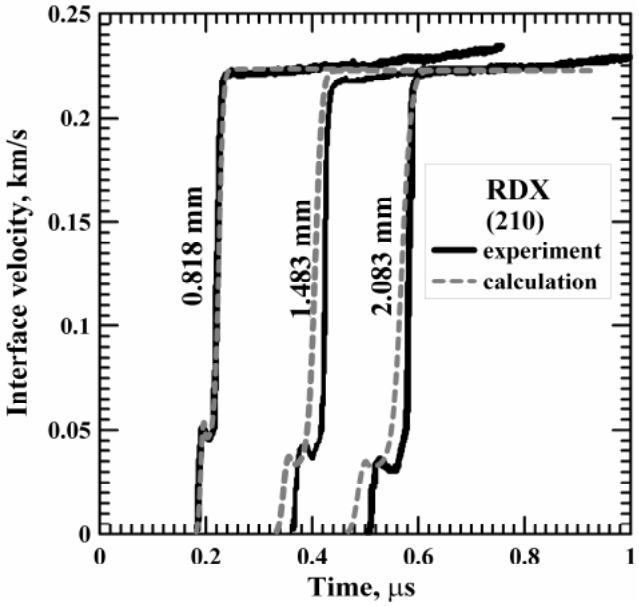

Figure 3: Time profiles of velocity of the boundary RDX/LiF at the loading along direction (210). Experimental data from [26] for various target thicknesses.

Simple one-term equation of state of RDX and LiF had been used in our simulations: $P = B \cdot (\rho - \rho_0)/\rho_0$, where ρ_0 is the normal density, B is the bulk modulus. We had found

for LiF: $B = 62$ GPa, $\rho_0 = 2.6$ g/cm^3, $G = 24.4$ GPa, and for RDX: $B = 27$ GPa, $\rho_0 = 1.866$ g/cm^3 and $G = 6$ GPa.

4 PLASTICITY OF ULTRAFINE-GRAINED AND NANOCRYSTALLINE METALS

In polycrystalline metals with large grains the different regions of the material have different orientation of lattice and of the dislocations slip systems. But boundaries don't effect on the dislocations motion till the dislocation range remain substantially lower than the grain diameter d. Decrease of the grain size, from the one hand, creates an additional resistance to the dislocation motion, which is described by the Hall-Petch relation [27,28] for the yield strength of the polycrystalline metals. From the other hand, it makes possible alternative mechanisms of plasticity. The grain boundary sliding can be an effective mechanism of plasticity in the ultrafine-grained ($d < 1$ μm) and nanocrystallin ($d < 0.1$ μm) metals [4-6].

Combined action of two plasticity mechanisms leads to a complicated behavior of the metal and to the complex dependence of the dynamical yield strength on the grain size, strain rate, temperature and origin dislocation density. If the origin dislocation density is high enough (the precise level depends on the stain rate), then the grain size dependence of the dynamical yield strength has one maximum in the nanocrystalline range of grain diameters. At large grain sizes the Hall-Petch relation takes place (the yield stress grows up with the diameter decrease); at smaller grain sizes the inverse Hall-Petch relation is observed [5]. Fig.4 shows an example of such situation: our calculation results [5] in comparison with the experimental data [29] and the molecular-dynamics simulations [30] are presented.

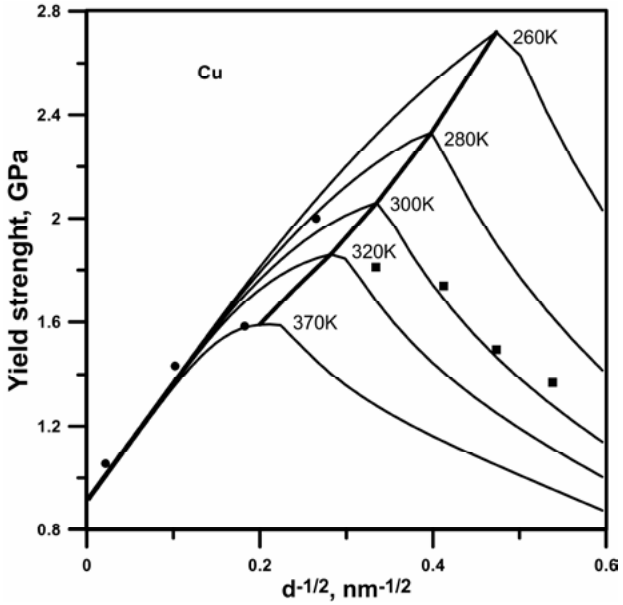

Figure 4: Dependence of the dynamical yield stress on the grain size for copper with high origin dislocation density. Markers correspond to experiments [29] (circles) and molecular dynamic simulations data [30] (squares); solid lines is our simulations at various temperature [5]. The strain rate is 0.5 ns^{-1}.

At low origin dislocation density or at high strain rate the second maximum appears in the

sub-micrometer range of the grain diameters. In this situation the inverse Hall-Petch relation takes place even for ultrafine-grained metals. Therefore, as the ultrafine-grained metal is harder than the coarse-grained one at the quasi-static loading, it becomes softer than the coarse-grained metal at the dynamical loading. Similar effects had been detected experimentally in tantalum [31] and copper [32].

5 LOCALIZATION OF PLASTIC FLOW

The described plasticity model has manifested itself as an effective tool for the numerical investigation of regularities of the plastic flow localization. Localization of the macroscopic plastic deformation is a widespread phenomenon in metals. It can be provoked by decrease of the material temperature, by increase of the deformation rate or by decrease of the grain size in polycrystalline metals. Local areas with high plastic deformation appear in the metal as a result of the localization. Classical viewpoint on this phenomenon proposes that a local temperature rise during the deformation leads to softening of the material, and that competition between the temperature softening and the strain hardening results in the plastic flow instability (the thermoplastic instability) and in the localization [33,34]. But for a large number of materials revealing the localization the plastic deformation results in inessential temperature increase, which is not enough for a substantial softening of the uniformly deformed material [35,36]. The high-speed infrared photography [37,38] have shown, that even in the areas of the plastic flow localization the temperature rise does not exceed 10 K in iron [37], while in titanium it is about 100 K [38]. Therefore, the thermoplastic instability could not be the universal mechanism of the localization.

We had numerically studied the simple shear of the perturbed samples of pure the monocrystalline aluminum, the aluminum-copper alloy [7] and the nanocrystalline aluminum. The pure aluminum is not inclined to the localization [39], while the aluminum alloys reveal it [40,41]. The main differences between the pure aluminum and the aluminum-copper alloy in our study were the higher value of the yield stress of the alloy and its decrease with temperature. Simple shear of 2D metallic sample with square cross-section was simulated. “Lower” face of the sample was at rest, while the “upper” face moved along the “lower” face with the constant velocity. Initial velocity was set linearly increasing from the “lower” face to the “upper” face, which corresponds to the uniform simple shear. Two different problems were determined by boundary conditions on the “side” faces: the constrained shear at the forced movement of the “side” faces and the free shear at free surface condition on it. The perturbed area was initially set in the form of horizontal narrow stripe with differing value of the temperature $T + \Delta T$, the dislocation density $\rho_{\mathrm{D}} + \Delta\rho_{\mathrm{D}}$ or the grain diameter d_1 in comparison with the rest of the material, where they were T, ρ_{D} and d correspondently.

Calculations have showed that initial perturbations of the dislocation density or temperature can lead to a restricted localization of the plastic flow along the perturbation, but they cannot initiate the plastic flow instability. The thermoplastic instability is restricted because the temperature perturbation of about 100 K is necessary for substantial localization, while the temperature rise at the plastic deformation is much less. In the case of the dislocation density perturbation the strain hardening restricts the localization degree.

Much more localization takes place at the free shear (Fig.5). Both in alloy and in the pure metal the localization begins along diagonals of the square without any initial perturbation of

the parameters; moreover, any perturbation of temperature or dislocation density does not effect in this case. The stress concentrators are the main factor of the plastic flow localization at the free shear and it is substantially more efficient than the perturbations of temperature or dislocation density (Fig.6). At the free shear the stress concentration takes place at the corners of the sample and produces the diagonal shear bands.

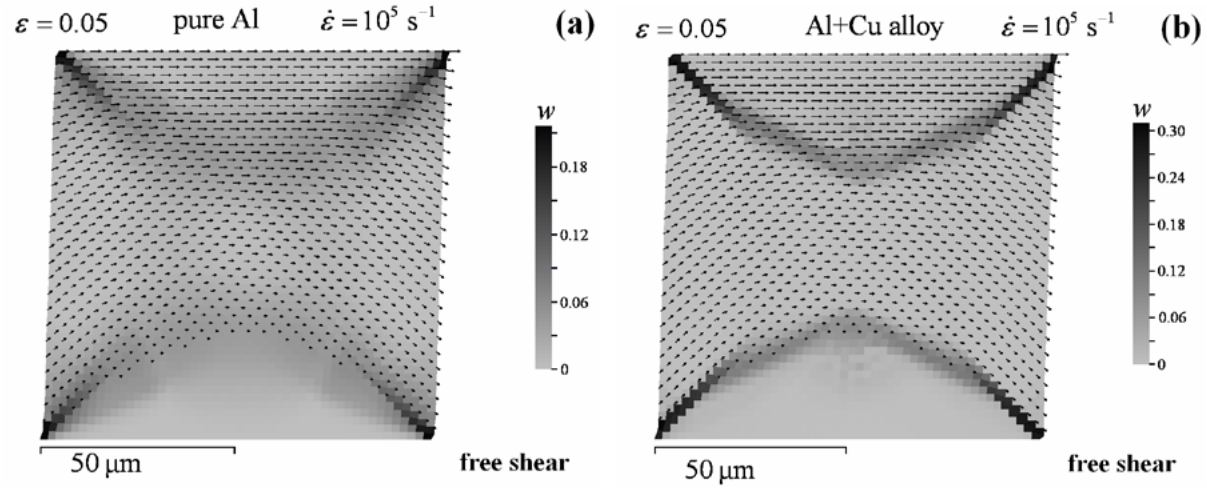

Figure 5: Distribution of the plastic strain intensity w in pure aluminum **(a)** and aluminum-copper alloy **(b)** at the free shear are presented at the total deformation of $\varepsilon = 0.05$. Both in alloy and in pure metal the localization begins along diagonals of the square. The region at rest near the "lower" face, the region moving with the constant velocity $\dot{\varepsilon} \cdot L$ near the "upper" face and the flowing central region appear as a result of development and intersection of the localization bands.

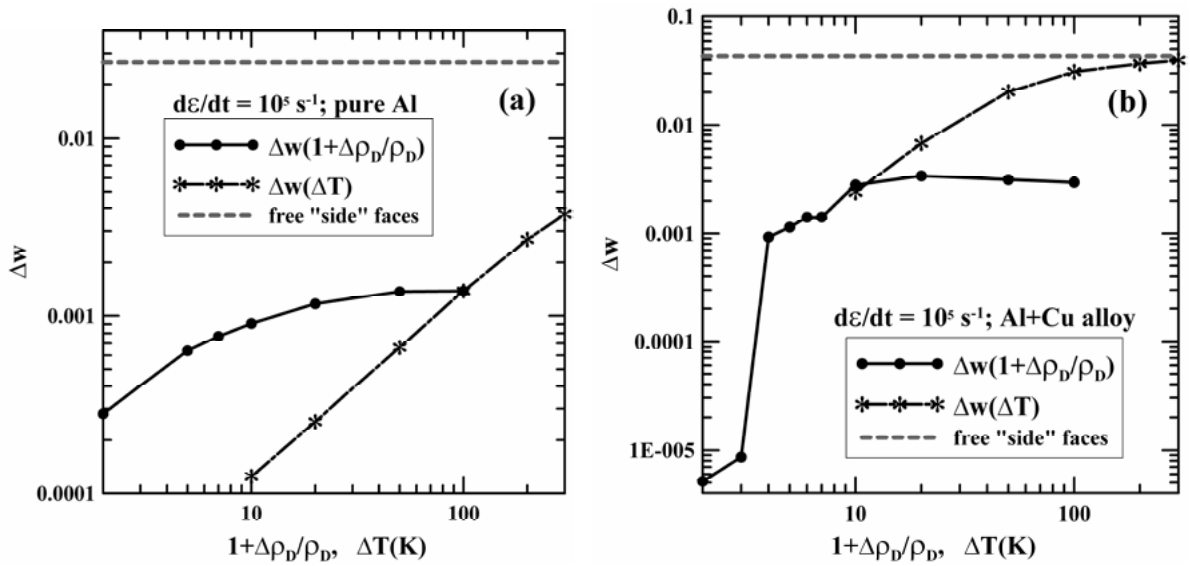

Figure 6: Comparison of the plastic flow localization degree ΔW produced by various initial perturbations of dislocation density or temperature at the constrained shear and the localization degree at the free shear. Shear deformation of pure aluminum **(a)** and aluminum-copper alloy **(b)**; the total strain is $\varepsilon = 0.05$. Values of the dislocation density perturbation and the temperature perturbation are presented on one axis. At the free shear (free "side" faces) the value of ΔW is approximately constant, therefore, it is represented by a horizontal line.

Perturbation of the grain size in the ultrafine-grained and the nanocrystalline aluminum leads to substantial localization of the plastic flow even at the "constrained" shear due to the difference in the dynamical yield strength. But the localization degree is all the same less than it at the "free" shear; they become comparable only at the grain size $d < 10\,\text{nm}$. It is remarkable that the localization degree in nanometals with the grain size $d < 100\,\text{nm}$ depends weakly on the perturbation value d_1 / d, therefore, the localization in such materials has to arise at any arbitrary size distribution of the grains.

6 CONCLUSIONS

In this report we have made a short overview of our work on the plasticity description through the kinetics of its elementary carriers (the dislocations, the grain boundaries) and of the obtained result in the related fields of research. The next conclusions can be formulated.

- The models of the dislocation plasticity and the grain boundary sliding are useful tools for description of the high-rate dynamical deformation of metals and molecular crystals because they take into account the inertness of plastic relaxation.
- At the initial stage of the elastic precursor formation its amplitude is close to the amplitude of the plastic shock wave even at the shock pressures of about 30 GPa. The precursor has the propagation velocity considerably higher than the longitudinal sound velocity; that allows precursor to run away from the plastic wave front.
- In the submicro- and nanocrystalline metals the combined action of the dislocation plasticity and the grain boundary sliding leads to complex dependence of the dynamical yield strength on the grain size, strain rate and temperature. At the strain rates above $10^6 s^{-1}$ the ultrafine-grained metals have the maximal dynamical yield strength instead of the nanocrystalline metals at the lower strain rates.
- Perturbation of the temperature, the dislocations density or the grain diameter leads to the restricted localization of the plastic flow, but it cannot initiate the plastic flow instability. The nonuniformity of acting stresses is the main factor of the plastic flow localization. Therefore, the process of localization must substantially depend on the loading conditions and on the internal structure of the material.

This study was supported by The Ministry of Education and Science of the Russian Federation (Agreement No. 14.B37.21.0384) and by the Russian Foundation for Basic Research (Projects Nos. 12-02-31375, and 12-02-13511).

REFERENCES

[1] Krasnikov, V.S., Kuksin, A.Yu., Mayer, A.E. and Yanilkin, A.V. Plastic deformation under high-rate loading: The multiscale approach. *Phys. Solid State* (2010)**52**(7):1386-1396.

[2] Krasnikov, V.S., Mayer, V.S. and Yalovets, A.P. Dislocation based high-rate plasticity model and its application to plate-impact and ultra short electron irradiation simulations. *Int. J. Plast.* (2011)**27**(8):1294-1308.

[3] Mayer, A.E., Khishchenko, K.V., Levashov, P.R. and Mayer, P.N. Modeling of plasticity and fracture of metals at shock loading. *J. Appl. Phys.* (2013)**113**(19):193508.

[4] Borodin, E.N., Mayer, A.E. and Krasnikov, V.S. Wave attenuation in microcrystal copper

at irradiation by a powerful electron beam. *Current Appl. Phys.* (2011)**11**(6):1315-1318.
[5] Borodin, E.N. and Mayer, A.E. Yield strength of nanocrystalline materials under high-rate plastic deformation. *Phys. Solid State* (2012)**54**(4):808-815.
[6] Borodin, E.N. and Mayer, A.E. A simple mechanical model for grain boundary sliding in nanocrystalline metals. *Mater. Sci. Eng. A.* (2012)**532**:245-248.
[7] Mayer, A.E., Borodin, E.N. and Mayer, P.N. Localization of plastic flow at high-rate simple shear. *Int. J. Plast.* (2013):in press (http://dx.doi.org/10.1016/j.ijplas.2013.05.005).
[8] Landau, L.D. and Lifshitz, E.M. *Course of Theoretical Physics*. Pergamon, New York, Vol. VI. (1987), Vol. VII (1986).
[9] Kolgatin, S.N. and Khachatur'yants, A.V. Interpolation equations of state of metals. *Teplofiz. Vys. Temp.* (1982)**20**:90-94.
[10] Fortov, V.E., Khishchenko, K.V., Levashov, P.R. and Lomonosov, I.V. Wide-range multi-phase equations of state for metals. *Nucl. Instrum. Meth. Phys. Res. A* (1998)**415**:604-608.
[11] Tallon, J.L. and Wolfenden, A. Temperature dependence of the elastic constants of aluminum. *J. Phys. Chem. Solids* (1979)**40**:831-837.
[12] Guinan, M.W. and Steinberg, D.J. Pressure and temperature derivatives of the isotropic polycrystalline shear modulus for 65 elements. *J. Phys. Chem. Solids* (1974)**35**:1501-1512.
[13] Wilkins, M.L. Calculation of elastic-plastic flow. UCRL-7322 (1963).
[14] Kosevich, A.M. Dynamical Theory of Dislocations. *Sov. Phys. Uspekhi* (1965)**7**:837-854.
[15] Al'shitz, V.A. and Indenbom, V.L. Dynamic dragging of dislocations. *Sov. Phys. Uspekhi* (1975)**18**:1-20.
[16] Yalovets, A.P. Calculation of flows of a medium induced by high-power beams of charged particles. *J. Appl. Mech. Tech. Phys.* (1997)**38**:137-150.
[17] Kanel, G.I., Razorenov, S.V. and Fortov, V.E. *Shock-Wave Phenomena and the Properties of Condensed Matter*. Springer, New York (2004).
[18] Kanel, G.I., Fortov, V.E. and Razorenov, S.V. Shock waves in condensed-state physics. *Phys. Usp.* (2007)**50**(7):771-791.
[19] Kanel, G.I., Razorenov, S.V., Baumung, K. and Singer, J. Dynamic yield and tensile strength of aluminum single crystals at temperatures up to the melting point. *J. Appl. Phys.* (2001)**90**(1):136-143.
[20] Kanel, G.I., Razorenov, S.V., Utkin, A.V. and Fortov, V.E. *Experimental Profiles of Shock Waves in Condensed Substances*. FIZMATLIT, Moscow, (2008).
[21] Ilnitski, D., Krasnikov, V., Kuksin, A., Mayer, A. and Yanilkin, A. Dynamics and kinetics of dislocations in metals and alloys under dynamic loading. *MRS Proceedings* (2013)**1535**:mmm12-a-0305 (http://dx.doi.org/10.1557/opl.2013.454).
[22] Mayer, A.E. and Krasnikov, V.S. Copper spall fracture under sub-nanosecond electron irradiation. *Eng. Fract. Mech.* (2011)**78**(6):1306-1316.
[23] Inogamov, N.A., Zhakhovskii, V.V., Khokhlov, V.A. and Shepelev, V.V. Superelasticity and the propagation of the shock waves in crystals. *JETP Lett.* (2011)**93**:226-232.
[24] Ashitkov, S.I., Agranat, M.B., Kanel, G.I., Komarov, P.S. and Fortov, V.E. Behavior of aluminum near an ultimate theoretical strength in experiments with femtosecond laser pulses. *JETP Lett.* (2010)**92**:516–520.
[25] Whitley, V.H., McGrane, S.D., Eakins, D.E., Bolme, C.A., Moore, D.S. and Bingert, J.F. The elastic-plastic response of aluminum films to ultrafast laser-generated shocks. *J. Appl. Phys.*

(2011)**109**:013505.
[26] Hooks, D.E., Ramos, K.J., Martinez, A.R., Elastic-plastic shock wave profiles in oriented single crystals of cyclotrimethylene trinitramine (RDX) at 2.25GPa. *J. Appl. Phys.* (2006)**100**:024908.
[27] Hall, E.O. The Deformation and Ageing of Mild Steel: III Discussion of Results. *Proc. Phys. Soc. B.* (1951)**64**:474-753.
[28] Petch, N.J. The cleavage strength of polycrystals. *J. Iron Steel Inst.* (1953)**174**:25-28.
[29] Siegel, R.W. and Fougere, G.E. Mechanical properties of nano- phase metals. *Nanostruct. Mater.* (1995)**6**:205-216.
[30] Kuksin, A.Yu., Stegailov, V.V. and Yanilkin, A.V. Atomistic simulation of plasticity and fracture of nanocrystalline copper under high-rate tension. *Phys. Solid State* (2008)**50**(11):2069-2075.
[31] Razorenov, S.V., Kanel, G.I., Garkushin, G.V. and Ignatova, O.N. Resistance to dynamic deformation and fracture of tantalum with different grain and defect structures. *Phys. Solid State* (2012)**54**(4):790-797.
[32] Dudarev, E.F., Markov, A.B., Bakach, G.P., Tabachenko, A.N., Polevin, S.D., Girsova, N.V., Kashin, O.A., Zhorovkov, M.F. and Rotshtein, V.P. Spall fracture of coarse- and ultrafine-grained FCC metals under nanosecond high-current relativistic beam irradiation. *Russ. Phys. J.* (2009)**52**(3):239–244.
[33] Bai, Y. and Dodd, B. *Shear Localization: Occurrence Theories and Applications.* Pergamon, Oxford (1992).
[34] Wright, T. *The Physics and Mathematics of Adiabatic Shear Bands.* Cambridge University Press, Cambridge (2002).
[35] Marchand, A. and Duffy, J. An experimental study of the formation process of adiabatic shear bands in a structural steel. *J. Mech. Phys. Solids* (1988)**36**:251–283.
[36] Rittel, D. and Wang, Z.G. Thermo-mechanical aspects of adiabatic shear failure of AM50 and Ti6Al4V alloys. *Mech. Mater.* (2008)**40**:629–635.
[37] Plekhov, O.A., Naimark, O.B., Saintier, N. and Palin-Luc, T. Elastic-plastic transition in iron: Structural and thermodynamic features. *Techn. Phys.* (2009)**54**:1141-1146.
[38] Plekhov, O., Chudinov, V., Leont'ev, V. and Naimark, O. Experimental investigations of the laws of energy dissipation during dynamic deformation of nanocrystalline titanium. Techn. Phys. Lett. (2009)**35**:92-95.
[39] Yellup, J.M. and Woodward, R.L. Investigaion into the prevention of adiabatic shear failure in high strength armor materials. *Res. Mech.* (1980)**1**:41–57.
[40] Chen, R.W. and Vecchio, K.S. Microstructural Characterization Of Shear Band Formation In Al-Li Alloys. *J. Phys. IV C* (1994)**8**:459–464.
[41] Bai, Y.L., Bai, J., Li, H.L., Ke, F.J. and Xia, M.F.Damage evolution, localization and failure of solids subjected to impact loading. *Int. J. Impact Engng.* (2000)**24**:685–701.